The effect of the flattening filter on photoneutron production at 10 MV in the Varian TrueBeam linear accelerator

Logan Montgomery[a)] and Michael Evans
Medical Physics Unit, McGill University, Montreal, QC H4A3J1, Canada

Liheng Liang
Medical Physics Unit, McGill University, Montreal, QC H4A3J1, Canada
Department of Radiation Oncology, Jewish General Hospital, Montreal, QC H3T1E2, Canada

Robert Maglieri and John Kildea
Medical Physics Unit, McGill University, Montreal, QC H4A3J1, Canada

(Received 26 April 2018; revised 25 July 2018; accepted for publication 8 August 2018; published 14 September 2018)

Purpose: Neutrons are an unavoidable by-product of high-energy radiation therapy treatments that deliver unwanted nontarget dose to patients. Use of flattening-filter-free (FFF) photon beams has been shown to significantly reduce photoneutron production per monitor unit (MU) of dose delivered. The purpose of this investigation was to characterize the photoneutron production of the 10 MV and 10 MV FFF beams of the Varian TrueBeam^{TM} linear accelerator.
Methods: Neutron fluence spectra were measured using a Nested Neutron Spectrometer^{TM} (NNS, Detec Inc., Gatineau, Canada). The ratios of neutron fluence and ambient dose equivalent for the 10 MV FFF beam relative to the 10 MV beam, dubbed FF-ratios (FFF/FF), were used to characterize the difference between the two beams. FF-ratios were compared under the following three conditions (a) per MU, at various locations in the treatment room, (b) per MU, with the linac jaws opened and closed, and (c) per electron striking the bremsstrahlung target, as opposed to per MU, at one location with the jaws closed.
Results: On average, the neutron fluence for the 10 MV FFF beam was 37% lower per MU than the 10 MV beam (FF-ratio = 0.63). The FF-ratio in neutron fluence and ambient dose equivalent did not vary by much between different locations within the treatment room. However, the FF-ratio in neutron ambient dose equivalent was reduced significantly when the linac jaws were opened compared to closed, which implies that the jaws contribute more to the photoneutron spectrum of the 10 MV FFF beam than to the 10 MV beam. Finally, it was found that the 10 MV FFF beam produces more photoneutrons per electron striking the bremsstrahlung target than the 10 MV beam (FF-ratio = 2.56).
Conclusions: The photoneutron fluence per MU produced by the 10 MV FFF beam is 37% lower than the 10 MV beam of a Varian TrueBeam linac. Accordingly, a reduction in neutron dose received by patients is achieved through use of the unflattened beam, provided that treatment plans for each beam require approximately the same number of MU. It was found to be instructive to compare the photoneutron yield per source electron between the two beams as it helped provide an understanding of the physics underlying photoneutron production in both beams. [https://doi.org/10.1002/mp.13148]

Key words: 10 MV, flattening filter-free, MLEM, neutron, TrueBeam

1. INTRODUCTION

During external beam radiation therapy treatments that utilize high-energy photons ($\gtrsim$ 8 MV), neutrons are produced via photoneutron reactions between photons and components inside the head of the linear accelerator (linac). Within the treatment room, the production of these unwanted but unavoidable photoneutrons poses a potential risk to both patients, in the form of nontarget dose,[1–3] and staff due to activation of in-room materials.[4–7] Compared to other types of ionizing radiation, neutrons have a high relative biological effectiveness for carcinogenesis that varies with neutron energy. Thus, treatment techniques that offer lower photoneutron yield, and thereby reduce the carcinogenic risk posed to patients by photoneutrons, are of interest to the radiation therapy community.

The primary sources of photoneutrons in a linac are the primary collimator, bremsstrahlung target, flattening filter, jaws, and the shielding material surrounding the bending magnet and head.[8–10] Flattening-filter-free (FFF) beams have been recently incorporated into clinical practice because they offer several advantages compared to conventional, flattened beams. These include the capability to deliver higher dose rates, reduce treatment duration, improve dosimetry, reduce photon leakage from the head, and reduce photoneutron yield.[11]

Measurements and Monte Carlo modeling have demonstrated that neutron yield per monitor unit (MU) is significantly reduced when the flattening filter is removed, but the overall shape of the neutron energy spectrum is essentially unchanged.[10,12–14] The first evidence of this was published in 2007 by Kry et al.[12], who measured the photoneutron fluence around a Varian 21EX Clinac with and without the flattening filter for an 18 MV beam. They noted that their 18 MV FFF beam used the same monitor chamber calibration as the 18 MV beam and delivered 3.65 cGy of photon dose at d_{max} in water along the central axis per MU, compared to 1 cGy for the 18 MV beam. An average reduction of 20% in the neutron fluence per MU was observed, corresponding to a 76% reduction in the neutron fluence per photon dose at d_{max}. Subsequently, they calculated that a reduction in neutron fluence by 69% could be expected for an IMRT prostate treatment plan delivered with their 18 MV FFF beam instead of the 18 MV beam.

Since the publication of Kry et al., there has been limited experimental data published on (a) modern linear accelerator models, such as the Varian TrueBeam, and on (b) 10 MV photon beams. Modern linacs are of interest because they offer the ability to treat patients using calibrated unflattened beams. 10 MV beams are of interest because they are the lowest energy photon beams at which photoneutron production is typically a concern. This is an important consideration, for example, when examining the implications of using 10 MV beams to treat patients with implanted cardiac devices. Additionally, IMRT treatments at 10 MV are of interest because of the potential for improved skin-sparing and deeper penetration than treatments at 6 MV.

Motivated by the above, we undertook an investigation to compare the relative photoneutron yield of the clinically commissioned 10 MV and 10 MV FFF beams of a Varian TrueBeam linear accelerator at our center. We used a Nested Neutron Spectrometer™ (NNS; Detec Inc., Gatineau Quebec)[15] to measure the photoneutron fluence spectra produced by each beam. To thoroughly examine the physics underlying photoneutron production, the following three measurement objectives were set:

1. Determine if the relative photoneutron yield per MU of the two beams varies with measurement location in the treatment room.
2. Evaluate the effect of the linac jaws on the relative photoneutron yield per MU of the two beams via measurements at two field sizes.
3. Determine which beam produces more photoneutrons per electron striking the linac bremsstrahlung target, and quantify by how much.

In this paper, we report on the methodology we used to achieve our three objectives and on the findings of our investigation. With regard to objective 2, we note that comparisons of the photoneutron yield of flattened and unflattened photon beams as a function of treatment field size have previously been reported in the literature.[10,12,16] Also, it is known that there is interplay between photoneutron production in the flattening filter for flattened beams and in the linac jaws for unflattened beams.[10] Our rationale for including a field-size comparison in this work was that it would facilitate understanding of the results of objective 3 given the potentially unique combination of flattening filter and jaws in the Varian TrueBeam at 10 MV.

2. MATERIALS AND METHODS

2.A. The nested neutron spectrometer

The NNS is a neutron spectrometer that operates similarly to a Bonner sphere spectrometer,[17] and was previously validated by our group for use in radiation therapy facilities.[18] It consists of a central He-3 detector and seven cylindrical high-density polyethylene moderator shells assembled in nesting Russian doll fashion. A schematic and photograph of the NNS are shown in Fig. 1. Thermal neutrons are detected by the He-3 detector through (n,p) reactions with the He-3 gas (Q-value 764 keV). The ambient neutron spectrum is sampled by surrounding the He-3 detector with moderator shells such that ambient neutrons of increasing energy are thermalized and become detectable as successive shells are added.

The He-3 detector can be operated in two modes: pulse-mode and current-mode. Pulse-mode, in which individual neutron events are counted, can only be reliably used in environments with count rates less than 1×10^4 counts per second (cps), and is thus unsuitable for use around radiation therapy linacs where neutron count rates may exceed 1×10^6 cps. For use in radiation therapy environments, the He-3 detector may be operated in current-mode, as described in our earlier publication.[18] In this mode, a neutron-insensitive He-4 detector is used to quantify any photon contribution to the He-3 signal. The resulting photon-subtracted accumulated charge measurements are converted to neutron count rates using a calibration coefficient of 7.0 fA/cps that was provided by the NNS vendor and previously validated by our group.[18]

In this paper, the term “measurement” will be used to describe a complete set of eight He-3 measurements obtained using all seven moderator configurations and the bare detector, with leakage and the photon component removed. For a particular experimental setup, one “measurement” gives rise to one measured spectrum for that setup after spectral unfolding, as described below.

2.B. Unfolding the neutron counts per second data

The count rates measured by the NNS for a particular moderator configuration represents a convolution of the ambient neutron fluence spectrum and the NNS response function for that configuration. To obtain the ambient neutron spectrum, the response functions must be unfolded from the cps data. In our research group, unfolding is performed using a custom-developed maximum-likelihood expectation–maximization (MLEM) algorithm that we

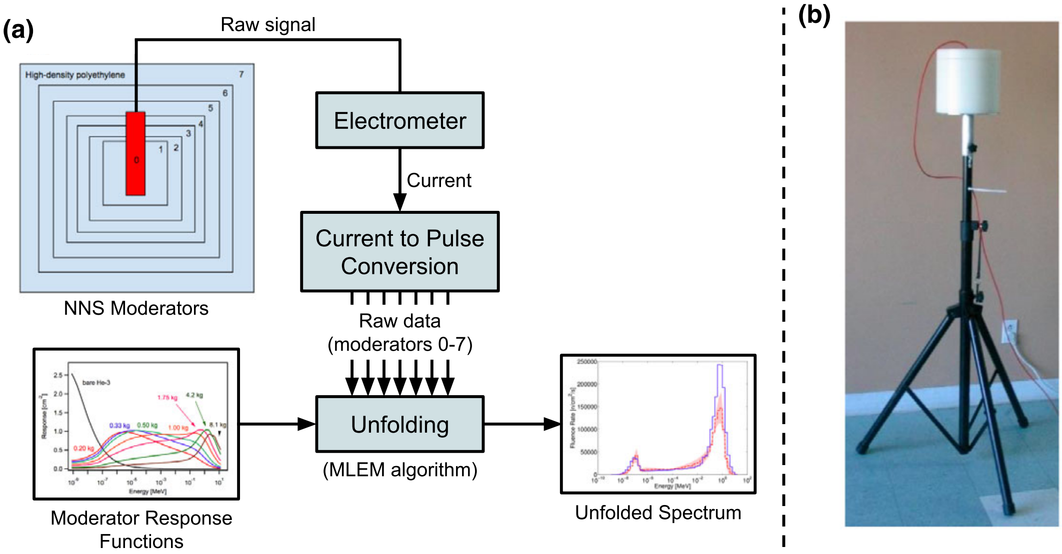

FIG. 1. The Nested Neutron Spectrometer^{TM} (NNS). (a) Schematic cross section of the cylindrical NNS system that shows the central He-3 detector (red, online version only) and seven moderator shells.[15] The signal processing pathway for current-mode operation is shown and includes moderator response functions that were generated by the NNS vendor. (b) Photograph of the NNS on a tripod. The tripod height may be adjusted between measurements to keep the He-3 detector at the same location for all moderator configurations. [Color figure can be viewed at wileyonlinelibrary.com]

validated in our earlier work using reference neutron sources and Monte Carlo modeling.[18] When iterated to convergence, the MLEM algorithm maximizes the likelihood of obtaining the measured data $\{m_i\}$ given that the spectrum is $\{n_j\}$, and is described as follows:

$$n_j^{k+1} = \frac{n_j^k}{\sum_{i=1}^{N} a_{ij}} \sum_{i=1}^{N} a_{ij} \frac{m_i}{\sum_{b=1}^{J} a_{ib} n_b^k}. \tag{1}$$

Here, the index i spans the number of moderator configurations (N), j and b span the number of energy bins (J) over which the NNS response functions are defined, and k is the iteration index of the MLEM algorithm. Thus, n^{k+1} is the next estimated spectrum of the MLEM algorithm, n^k is the current estimate, a is the response function of the detector, and m is the set of measurements in counts per second. The NNS response functions span thermal to fast neutron energies as shown in Fig. 1, and thus permit unfolding the entire neutron spectrum of interest in radiation therapy. A step function (high at thermal energies and low onward) is used as the starting spectrum for the unfolding process. Its appropriateness was determined by reconstructing Monte Carlo spectra, as outlined in our previous publication.[18]

A stopping criterion must be provided to the MLEM algorithm to terminate the unfolding process. To this end, a number of iterations must be identified that yields completely unfolded spectra with minimal accumulation of noise. In this work, in order to ensure fair comparison between the FF and FFF beams, the same number of iterations was used for all corresponding 10 MV and 10 MV FFF spectra that were measured under identical experimental conditions.

In our unfolding algorithm, uncertainties in the unfolded spectra are estimated using a Poisson random sampling process. Each count rate measurement is considered as the mean and variance of a Poisson distribution, from which a randomly sampled measurement may be obtained. Fifty randomly sampled measurements are obtained in this way and each is unfolded to obtain 50 sampled neutron spectra. The average root mean square difference between the measured spectrum and the sampled spectra is used as the spectrum uncertainty.

2.C. Facilities and experimental setup

Two photon beams of a Varian TrueBeam linac were used in this study; the 10 MV and 10 MV FFF beams. Both beams were in clinical use, having been commissioned and calibrated in accordance with the AAPM TG-51 protocol such that one MU corresponds to a photon dose delivery of 1 cGy at d_{max} in water on the central axis for a field size of 10×10 cm^2.[19] All measurements were obtained with gantry rotation of 0°, collimator rotation of 0°, couch rotation of 0°, and a fully retracted multileaf collimator. The sensitive volume of the detector within the NNS was placed at the height of isocenter at for all measurements.

2.C.1. Setup for objective 1

The first measurement objective was to determine if the relative photoneutron yield per MU between the two beams is dependent on measurement location within the treatment room. Thus, neutron spectral measurements were made for each beam with the NNS placed at three distinct locations: location A at 100 cm from isocenter along the couch and away from the gantry, location B at 200 cm from isocenter also along the couch and away from the gantry, and location C at the maze-room junction. These locations are shown in Fig. 2. The linac jaws were closed (field size of 0.5×0.5 cm^2 at isocenter) and a photon dose rate of

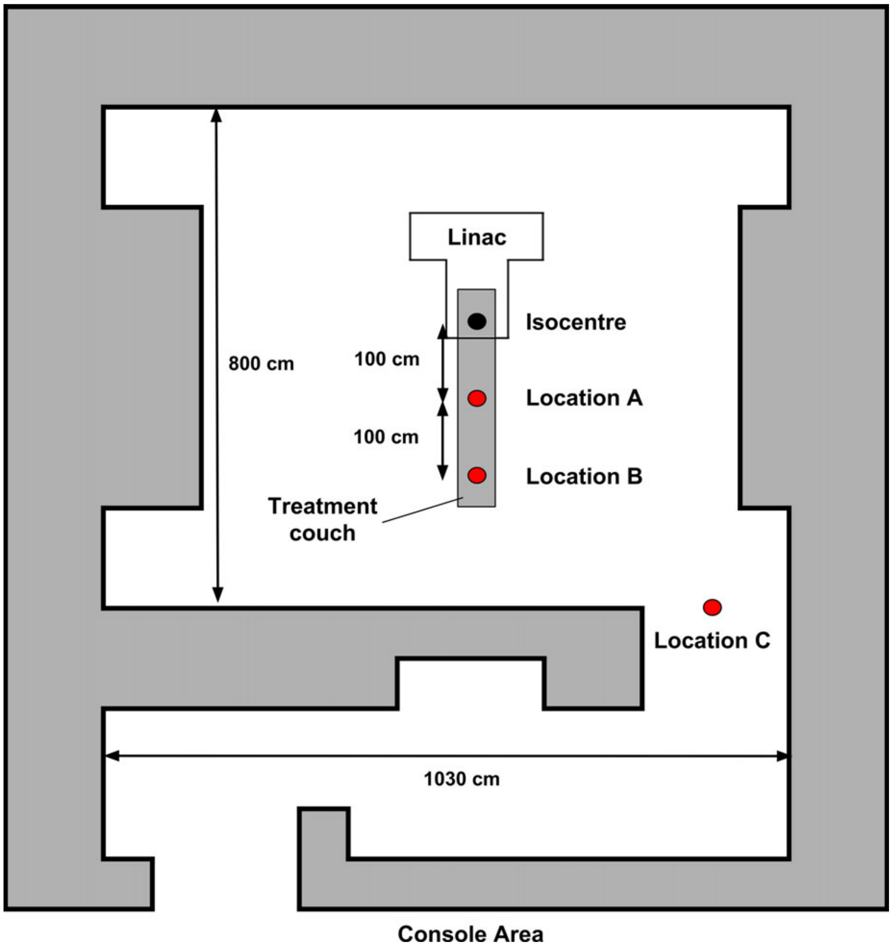

FIG. 2. Schematic of the doorless treatment room in which neutron spectral measurements were made. Measurement locations are shown in red (online version only). Figure not to scale. [Color figure can be viewed at wileyonlinelibrary.com]

400 MU/min was used to deliver 200 MU for each of the eight NNS configurations. For simplicity, the same dose rate was used for the two beams.

2.C.2. Setup for objective 2

The second objective was to evaluate the effect of the linac jaws on the relative photoneutron yield of the two beams. Therefore, an additional measurement was made at location A for both beams with open jaws (field size of 20×20 cm^2) to be compared with those acquired at location A with the jaws closed. The dose rate of 400 MU/min and dose of 200 MU were maintained for this measurement.

2.C.3. Setup for objective 3

The third and final objective was to determine which beam produces more photoneutrons per electron striking the linac's bremsstrahlung target (i.e., per source electron). An oscilloscope was used to measure the electron pulse width and pulse repetition frequency on the target in order to find dose rates at which the rate of source electrons was the same for both beams. We found that when operated at their maximum dose rates with the dose rate servo turned off, the rates of source electrons were the same. These dose rates were nominally 600 MU/min for the 10 MV beam and 2400 MU/min for the 10 MV FFF beam but they ran approximately 15% higher when the dose rate servo was turned off.

To meet our third objective, measurements were made with the NNS at location A while both beams were operated at their maximum dose rates with the dose rate servo turned off and linac jaws closed. We operated them for the same amount of time (30 s for each NNS configuration) to generate the same number of source electrons for each beam.

2.D. Measurement quantities

The counts per second data for each measurement were unfolded to obtain a neutron fluence spectrum. The total fluence (Φ) for each measurement was calculated by integrating over the entire unfolded spectrum. For objectives 1 and 2, in which the same number of MU was used for both the FFF and FF beams, the neutron fluence was normalized per MU. For objective 3, since the absolute number of source electrons for each beam was unknown but equal, the neutron fluence for each beam was normalized per second.

The neutron ambient dose equivalent (H^* (10)) was also calculated for each measurement. This was achieved by multiplying the measured fluence in each energy bin of the neutron fluence spectrum by the appropriate neutron fluence-to-dose conversion coefficient provided in ICRP-74,[20] and summing over each bin.

To examine the effect of the flattening filter, the ratio in measured quantities of the FFF to the FF beam, which we refer to as the FF-ratio (FFF/FF), was calculated for all measurements. Statistical uncertainties in all measurement quantities were calculated by propagating the uncertainty in the unfolded spectra using standard error propagation rules.

3. RESULTS

3.A. Results for objective 1: Effect of measurement location on photoneutron yield per MU

The unfolded neutron fluence spectra per MU for the 10 MV and 10 MV FFF beams that were measured at locations A, B, and C are shown in Fig. 3. Statistical uncertainties are shown as shaded regions around the spectra. A fast neutron peak and thermal neutron peak are seen for both beams under all setup conditions. The total neutron fluence and ambient dose equivalent per MU, as determined from the spectra, are tabulated in Tables I and II. The FF-ratios in these parameters are also provided. It is evident from Fig. 3 and Table I that the neutron fluence per MU for the 10 MV FFF beam was consistently lower than the 10 MV beam.

As expected, the total neutron fluence per MU decreased with increasing distance from the linac for both the flattened and unflattened beam. A statistically significant decrease in the FF-ratio at location C compared to locations A and B was observed. This may be attributed to the almost-complete thermalization of the fast neutron peak of the unflattened beam as seen in Fig. 3(d).

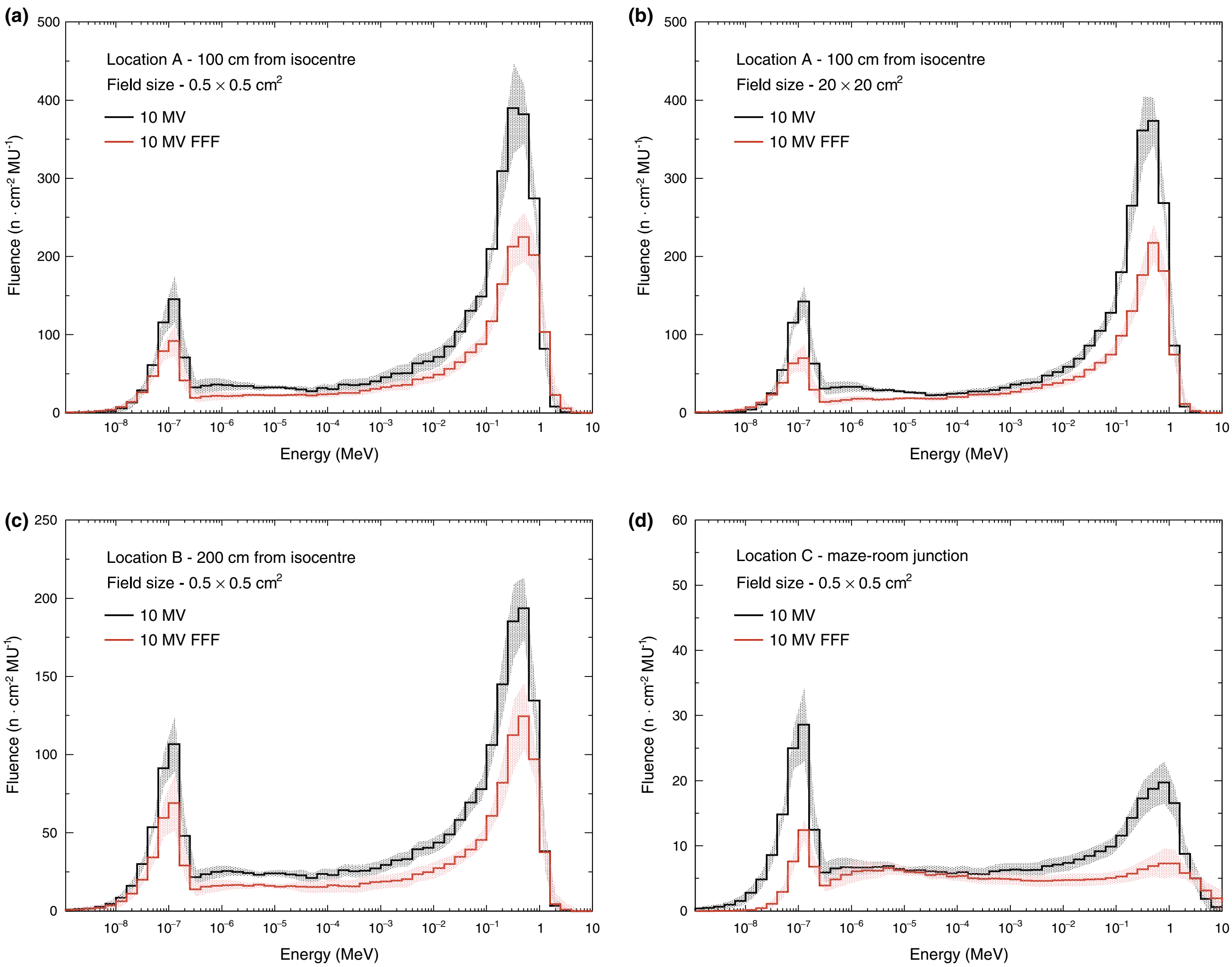

FIG. 3. Neutron fluence spectra per MU for the 10 MV (black) and 10 MV FFF (red, online version only) beams of a Varian TrueBeam linac. Spectra were measured at (a) location A, 100 cm from isocenter along the couch and away from the gantry, with closed linac jaws (field size of 0.5 × 0.5 cm^2), (b) location A, with open linac jaws (field size of 20 × 20 cm^2), (c) location B, 200 cm from isocenter along the couch and away from the gantry, with closed linac jaws, and (d) location C, the maze-room junction with closed linac jaws. Statistical uncertainties are shown as shaded regions around each spectrum. [Color figure can be viewed at wileyonlinelibrary.com]

TABLE I. Total neutron fluence per monitor unit (Φ) for the 10 MV and 10 MV FFF beams of the Varian TrueBeam linac.

Location	Field size (cm^2)	Φ($n\ cm^{-2}\ MU^{-1}$)		Φ_{FFF}/Φ_{FF}
		10 MV	10 MV FFF	
A	0.5 × 0.5	$(3.52 \pm 0.08) \times 10^3$	$(2.32 \pm 0.07) \times 10^3$	0.66 ± 0.02
A	20 × 20	$(3.13 \pm 0.08) \times 10^3$	$(1.94 \pm 0.07) \times 10^3$	0.62 ± 0.03
B	0.5 × 0.5	$(2.08 \pm 0.07) \times 10^3$	$(1.33 \pm 0.05) \times 10^3$	0.64 ± 0.03
C	0.5 × 0.5	$(4.0 \pm 0.1) \times 10^2$	$(2.36 \pm 0.09) \times 10^2$	0.58 ± 0.03

TABLE II. Neutron ambient dose equivalent per monitor unit ($H^*(10)$) for the 10 MV FFF beams of the Varian TrueBeam linac.

Location	Field size (cm^2)	H^* (10) (mSv MU^{-1})		$H^*(10)_{FFF}/H^*(10)_{FF}$
		10 MV	10 MV FFF	
A	0.5 × 0.5	$(4.1 \pm 0.1) \times 10^{-4}$	$(2.86 \pm 0.09) \times 10^{-4}$	0.69 ± 0.03
A	20 × 20	$(3.90 \pm 0.08) \times 10^{-4}$	$(2.41 \pm 0.07) \times 10^{-4}$	0.62 ± 0.02
B	0.5 × 0.5	$(2.05 \pm 0.07) \times 10^{-4}$	$(1.38 \pm 0.06) \times 10^{-4}$	0.67 ± 0.04
C	0.5 × 0.5	$(3.7 \pm 0.2) \times 10^{-5}$	$(2.0 \pm 0.2) \times 10^{-5}$	0.55 ± 0.06

The change in neutron ambient dose equivalent per MU as a function of location, as tabulated in Table II, was found to be consistent with the change in fluence for both beams.

3.B. Results for objective 2: Effect of the linac jaws on photoneutron yield per MU

Whether the jaws were opened or closed had an observable effect on the measured quantities. As shown in Table I, the FF-ratio in neutron fluence was lower with open jaws than closed jaws at location A, although the two values were within statistical uncertainty. The FF-ratio in neutron ambient dose equivalent per MU was also lower with open jaws, as shown in Table II, but the reduction was statistically significant in this case.

3.C. Results for objective 3: Photoneutron yield per source electron

The unfolded neutron fluence rate spectra obtained at location A for the 10 MV and 10 MV FFF beams with an equal number of source electrons are shown in Fig. 4. For comparison, the spectra obtained using 400 MU/min at location A with closed linac jaws were renormalized per unit time and are also plotted in Fig. 4.

The FF-ratios in the fluence rate and ambient dose equivalent rate for the two beams with equal source-electron rates were determined to be $\frac{\dot{\Phi}_{FFF}}{\dot{\Phi}_{FF}} = 2.56 \pm 0.05$ and $\frac{(\dot{H}^*(10))_{FFF}}{(\dot{H}^*(10))_{FF}} = 2.64 \pm 0.05$, respectively. We note that these FF-ratios per source electron are approximately four times larger than the FF-ratios per MU, for which both beams were operated at 400 MU/min at location A. This was expected given the relative increase in dose rate from 400 MU/min to the maximum for each beam $(\frac{400\,\mathrm{MU/min}}{400\,\mathrm{MU/min}}$ to $\frac{2400\,\mathrm{MU/min}}{600\,\mathrm{MU/min}})$.

4. DISCUSSION

To evaluate the consistency of our measured photoneutron yield with existing published data, we compared our neutron ambient dose equivalent measurement at location A with closed linac jaws using the 10 MV beam to the data reported for the 10 MV beam of a Varian Clinac in NCRP 151 at the same location.[21] Our measured value of $(4.1 \pm 0.1) \times 10^{-4}$ mSv/MU corresponds to (41 ± 1) µSv/Gy, which agrees with the published value of 40 µSv/Gy.

4.A. Photoneutron yield per MU for the 10 MV and 10 MV FFF beams

In this investigation, it was found that the photoneutron fluence per MU produced by a Varian TrueBeam linac was 34%–42% lower for the 10 MV FFF beam than the 10 MV beam. This reduction in neutron fluence per MU for the clinically commissioned and calibrated unflattened beam is due to the reduction in upstream photon fluence required to produce an MU when the attenuating effect of the flattening filter is removed.[12] Qualitatively, this is consistent with previous experimental and Monte Carlo studies at various photon beam energies for various linac models.[10,12–14] The closest point of reference to the present investigation was an abstract published in 2015 by Sawkey and Svatos who simulated the neutron fluence produced by the 10 MV FFF and 10 MV beams of a Varian TrueBeam over a 70 cm radius sphere centered on the linac head.[13] They measured an FF-ratio in neutron fluence per MU of 0.58, which agrees well with our results tabulated in Table I.

Corresponding to the lower neutron fluence for the 10 MV FFF beam, a reduction in neutron ambient dose equivalent of 31%–38% was observed at the patient-relevant locations A and B. To assess the potential reduction in neutron dose received by patients through use of the 10 MV FFF beam instead of the 10 MV beam, one must consider the number of

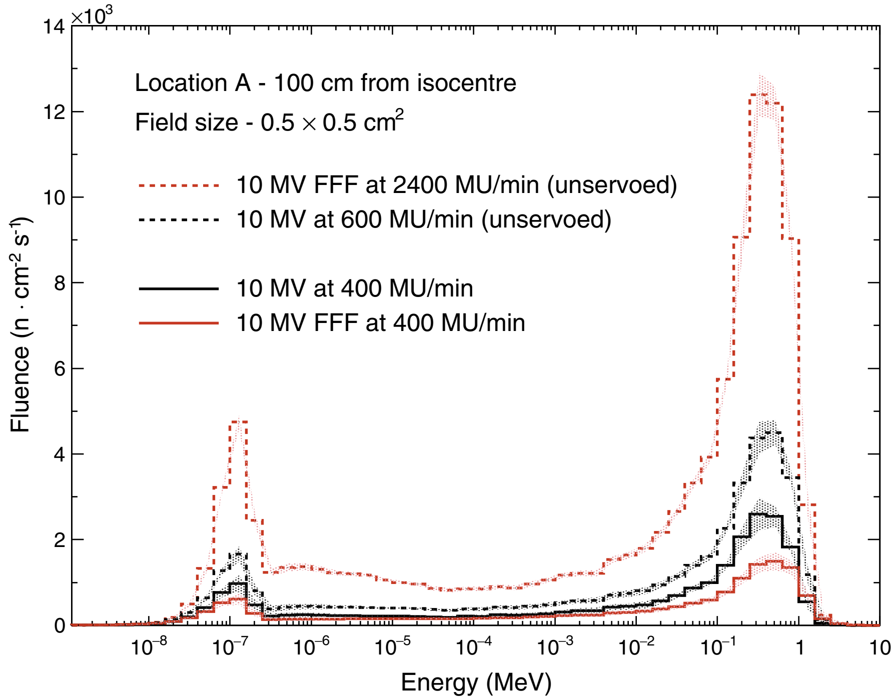

FIG. 4. Neutron fluence rate spectra for the 10 MV (black) and 10 MV FFF (red, online version only) beams of a Varian TrueBeam linac measured at location A, 100 cm from isocenter along the couch and away from the gantry with linac jaws closed. The spectra depicted with dashed lines correspond to an equal number of source electrons and were obtained using the maximum available dose rate of each beam. The spectra depicted with solid lines correspond to an equal number of MU and were presented in Fig. 3(a). Statistical uncertainties are shown as shaded regions around each spectrum. [Color figure can be viewed at wileyonlinelibrary.com]

MU required to deliver clinically equivalent treatment plans for the two beams. Chung et al.[22] compared the number of MU required for equivalent VMAT-SABR (volumetric-modulated arc therapy, stereotactic ablative body radiation therapy) prostate treatment plans using 10 MV and 10 MV FFF beams. They found that the 10 MV FFF plans required 10% more MU than the 10 MV plans on average. Similarly, Stieler et al.[23] found that 8% more MU were required for 6 MV FFF VMAT plans than 6 MV plans to treat multiple brain metastases. However, they also found that 2%–4% fewer MU were required for 6 MV FFF IMRT plans than 6 MV plans to treat single brain metastases. Based on a review of the literature, they concluded that flattening-filter-free treatment plans for large volumes or complex plans tend to require more MU than equivalent plans with flattened beams.

Thus, it seems reasonable to expect that approximately the same number or slightly more MU (on the order of 10%) are required for 10 MV FFF treatment plans than 10 MV plans. This does not offset the 31%–38% reduction in neutron ambient dose equivalent per MU for the 10 MV FFF beam at locations A and B. An important reduction in neutron dose received by patients treated with the 10 MV FFF beam can therefore be expected, although consideration must be given to the size of the treatment volume and plan complexity. Additionally, the increase in scattered and leakage photon dose associated with a plan that requires more MU must be considered in order to fully account for the nontarget dose received by patients.

4.B. The effect of measurement location on photoneutron yield per MU

Changes to both the unflattened and flattened photoneutron fluence spectra as the NNS was placed further from the linac were qualitatively similar to previous findings by our group at 18 MV.[18] The total neutron fluence for each beam decreased with increasing displacement from isocenter, and the dominant peak in the spectrum transitioned from the fast peak at location A, 100 cm from isocenter, to the thermal peak at location C, at the maze-room junction. This change in the dominant peak of the spectra for both beams was due to thermalization of fast neutrons by the treatment room walls and furnishings.[24] The FF-ratios did not change significantly from one location to the next for all measured quantities. This is consistent with findings in the literature at 10, 15, and 18 MV for measurement locations outside of the treatment field.[12,14]

4.C. The effect of the linac jaws on photoneutron yield per MU

Neutron fluence and ambient dose equivalent were found to decrease slightly more for the unflattened beam than the flattened beam when the linac jaws were opened compared to when they were closed. Although the reduction observed in the FF-ratio for the neutron fluence was within statistical uncertainty, the reduction in the FF-ratio for the neutron ambient dose equivalent was found to be statistically significant. The reduction may be attributed to the fact that the neutron fluence to ambient dose conversion coefficients are energy dependent and exhibit a peak around 1 MeV.[20] As seen in Figs. 3(a) and 3(b), the fast peak of the flattened spectrum shifted closer to 1 MeV (from 0.25 to 0.4 MeV) when the jaws were opened compared to when the jaws were closed, while the peak of the unflattened spectrum remained at the same energy.

Physically, this may be explained by examining the relative amount of neutrons produced by the various the components of the linac head. Kry et al.[10] demonstrated, using Monte Carlo modeling, that the linac jaws contribute more to the neutron yield of the unflattened beam than the flattened beam at 18 MV for the Varian 21EX Clinac.[10] This is because without a flattening filter to attenuate the upstream photons, the full neutron-producing potential of the photon beam, which would otherwise be reduced by neutron production in the flattening filter, is transported to the jaws. The jaws thus play a more important role in generating neutrons for the unflattened beam than the flattened beam. This finding is of particular relevance when interpreting the photoneutron yield per source electron.

4.D. Photoneutron production per source electron

The photoneutron fluence per source electron obtained for the 10 MV FFF beam was 2.56 times greater than for the 10 MV beam. Qualitatively similar findings have been reported for 18 MV and 18 MV FFF photon beams by other groups.[10,16] When the rate of electrons striking the bremsstrahlung target is the same, the difference in photoneutron fluence between the flattened and unflattened beam is simply due to the presence of the flattening filter. Everything else, including the photon fluence upstream of the flattening filter, remains the same. This manifests itself as higher photoneutron production per source electron for the unflattened beam than the flattened beam for two reasons, both of which arise from the fact that the jaws contribute more to photoneutron production in the unflattened beam.

First, the jaws are further downstream in the linac head than the flattening filter. Therefore, neutrons produced in the jaws are less likely to be absorbed before exiting the linac than those produced in flattening filter. Second, the material composition of a flattening filter is typically different than that of the jaws,[10,14] with the jaws having a higher photonuclear cross-section. For example, Najem et al.[14] reported that the 10 MV flattening filter of the Varian Clinac is composed of copper, while linac jaws are typically composed primarily of tungsten.[12] The photoneutron cross-section of tungsten has a threshold energy below 10 MeV and is larger than the cross-section of most intermediate-Z metals like copper, which have a threshold energy around 10 MeV.[25] While the material compositions of the TrueBeam's 10 MV flattening filter and jaws are not disclosed by the vendor, we can use the observations from other linac models by the same vendor to postulate that the jaws produce more photoneutrons per photon than the flattening filter in a 10 MV beam.

Although it is of no clinical consequence, we believe that our approach of examining the relative photoneutron production per source electron helps elucidate the underlying physics of photoneutron production in linacs, and allows for comparison of findings obtained using different linacs and different MU calibrations.

5. CONCLUSIONS

The photoneutron production of a Varian TrueBeam linear accelerator was investigated at 10 MV with and without a flattening filter using a Nested Neutron Spectrometer. It was found that the neutron fluence per MU of the unflattened beam was 34%–42% lower than the flattened beam, with minor variation as a function of measurement location and jaw setting. Thus, an important reduction in the neutron dose received by patients can be achieved through use of the 10 MV FFF beam compared to the 10 MV beam, provided that treatment plans for each beam require approximately the same number of MU.

When examined from the perspective of the number of neutrons produced per electron striking the bremsstrahlung target, it was found that the 10 MV FFF beam actually produces 2.56 times more neutrons per source electron than the 10 MV beam. This difference may be attributed to the composition of the jaws and the higher contribution of the jaws to the photoneutron fluence of the unflattened beam than the flattened beam.

ACKNOWLEDGMENTS

We acknowledge the support of the Natural Sciences and Engineering Research Council of Canada (NSERC) (Alexander Graham Bell Canada Graduate Scholarship-Doctoral: L. Montgomery, Discovery Grant: J. Kildea). Partial support for this research was provided by the CREATE Medical Physics Research Training Network grant of the Natural Sciences and Engineering Research Council (Grant number: 432290) and by the Canadian Nuclear Safety Commission (support for student Robert Maglieri). The Nested Neutron Spectrometer used in this investigation was generously provided on loan from the Canadian Nuclear Safety Commission (CNSC). Helpful advice and discussions provided by Stephen Davis (McGill), Susannah Hickling (McGill), Joe Larkin (McGill University Health Centre), Angel Licea (CNSC), and Jacques Dubeau (Detec Inc.) are gratefully acknowledged.

CONFLICTS OF INTEREST

The authors have no relevant conflicts of interest to disclose.

[a]Author to whom correspondence should be addressed. Electronic mail: logan.montgomery@mail.mcgill.ca.

REFERENCES

1. Kry SF, Bednarz B, Howell RM, et al. AAPM TG 158: measurement and calculation of doses outside the treated volume from external-beam radiation therapy. *Med Phys*. 2017;44:e391–e429.

2. Newhauser WD, Durante M. Assessing the risk of second malignancies after modern radiotherapy. *Nat Rev Cancer*. 2011;11:438–448.
3. Kry SF, Salehpour M, Followill DS, et al. The calculated risk of fatal secondary malignancies from intensity-modulated radiation therapy. *Int J Radiat Oncol Biol Phys*. 2005;62:1195–1203.
4. Wang YZ, Evans MD, Podgorsak EB. Characteristics of induced activity from medical linear accelerators. *Med Phys*. 2005;32:2899–2910.
5. Fischer HW, Tabot B, Poppe B. Comparison of activation products and induced dose rates in different high-energy medical linear accelerators. *Health Phys*. 2008;94:272–278.
6. Polaczek-Grelik K, Karaczyn B, Konefal A. Nuclear reactions in linear medical accelerators and their exposure consequences. *Appl Radiat Isot*. 2012;70:2332–2339.
7. Rawlinson JA, Islam MK, Galbraith DM. Dose to radiation therapists from activation at high-energy accelerators used for conventional and intensity-modulated radiation therapy. *Med Phys*. 2002;29:598–608.
8. Mao X, Kase K, Liu J, Nelson W, Kleck J, Johnsen S. Neutron sources in the Varian Clinac 21000/23000 medical accelerator calculated by the EGS4 code. *Health Phys*. 1997;72:524–529.
9. Zanini A, Durisi E, Fasolo F, et al. Monte carlo simulation of the photoneutron field in linac radiotherapy treatments with different collimation systems. *Phys Med Biol*. 2004;49:571–582.
10. Kry SF, Howell RM, Titt U, Salehpour M, Mohan R, Vassiliev ON. Energy spectra, sources, and shielding considerations for neutrons generated by a flattening filter-free clinac. *Med Phys*. 2008;35:1906–1911.
11. Georg D, Knöös T, McClean B. Current status and future perspective of flattening filter free photon beams. *Med Phys*. 2011;38:1280–1293.
12. Kry SF, Titt U, Ponisch F, et al. Reduced neutron production through use of a flattening-filter-free accelerator. *Int J Radiat Oncol Biol Phys*. 2007;68:1260–1264.
13. Sawkey D, Svatos M. Su-e-t-168: Characterization of neutrons from the TrueBeam treatment head. In: *Fifty-seventh annual meeting of the American association of physicists in medicine, vol. 42*. American Association of Physicists in Medicine; 2015:3370.
14. Najem MA, Abolaban FA, Podolyák Z, Spyrou NM. Neutron production from flattening filter free high energy medical linac: a Monte Carlo study. *Radiat Phys Chem*. 2015;116:176–180.
15. Dubeau J, Hakmana Witharana SS, Atanackovic J, Yonkeu A, Archambault JP. A neutron spectrometer using nested moderators. *Radiat Prot Dos*. 2012;150:217–222.
16. Mesbahi A. A Monte Carlo study on neutron and electron contamination of an unflattened 18-MV photon beam. *Appl Radiat Isot*. 2009;67:55–60.
17. Bramblett RL, Ewing RI, Bonner TW. A new type of neutron spectrometer. *Nucl Instrum Methods*. 1960;9:1–12.
18. Maglieri R, Licea A, Evans M, Seuntjens J, Kildea J. Measuring neutron spectra in radiotherapy using the nested neutron spectrometer. *Med Phys*. 2015;42:6162–6169.
19. Almond PR, Biggs PJ, Coursey B, et al. AAPM's TG-51 protocol for clinical reference dosimetry of high-energy photon and electron beams. *Med Phys Lancast*. 1999;26:1847–1870.
20. International Commission on Radiological Protection. Conversion coefficients for use in radiological protection against external radiation. Tech. Rep. ICRP Publication 74, International Organization for Standardization; 1996.
21. National Council on Radiation Protection and Measurements. Structural shielding design and evaluation for megavoltage x- and gamma-ray radiotherapy facilities. *NCRP Report*, no. 151; 2006.
22. Chung J, Kim J, Eom K, et al. Comparison of VMAT-SABR treatment plans with flattening filter (FF) and flattening filter filter-free (FFF) beam for localized prostate cancer. *J Appl Clin Med Phys*. 2015;16:302–313.
23. Stieler F, Fleckenstein J, Simeonova A, Wenz F, Lohr F. Intensity modulated radiosurgery of brain metastases with flattening filter-free beams. *Radiother Oncol*. 2013;109:448–451.
24. Pena J, Franco L, Gómez F, Iglesias A, Pardo J, Pombar M. Monte Carlo study of Siemens PRIMUS photoneutron production. *Phys Med Biol*. 2005;50:5921–5933.
25. International Atomic Energy Agency. Handbook on photonuclear data for applications cross-sections and spectra. Tech. rep., IAEA-TECDOC-1178; March 2000.

RIT®

RIT IS YOUR BEST SOURCE FOR MACHINE QA SOFTWARE SOLUTIONS DESIGNED FOR ACCURAY® USERS.

RADIXACT® TG-148 QA

A comprehensive test suite for helical TomoTherapy® and Radixact® machines, in accordance with TG-148

Designed with the TG-148 report in mind, RITG148+ analyzes the standardized machine QA tests for TomoTherapy® and Radixact® machines, including Static & Rotational Output Consistency, Jaw Centering and Alignment, Overhead Laser Positioning, Interrupted Treatment, and all others recommended for daily, monthly, and annual QA. RITG148+ also analyzes image quality using the Tomotherapy Cheese phantom.

CYBERKNIFE® TG-135 QA

A comprehensive test suite for CyberKnife® and all robotic radiosurgery, in accordance with TG-135

RITG135 contains five fully-automated QA tests for CyberKnife® machines: End-to-End Test, AQA Test, Iris Test, Laser Coincidence, and M6 MLC (Garden Fence) Test. RITG135 was designed to simplify and enhance current methods for performing these routine tasks. Combining a user-friendly interface with automated film detection algorithms, the software eliminates the need for manual image manipulation, increasing your efficiency.

ALL-IN-ONE MACHINE QA

RIT *Complete*

In addition to full CyberKnife® and TomoTherapy® QA, RIT *Complete* provides comprehensive QA for TG-142. This package features all of RIT's innovative therapy products, making it the all-in-one software solution.

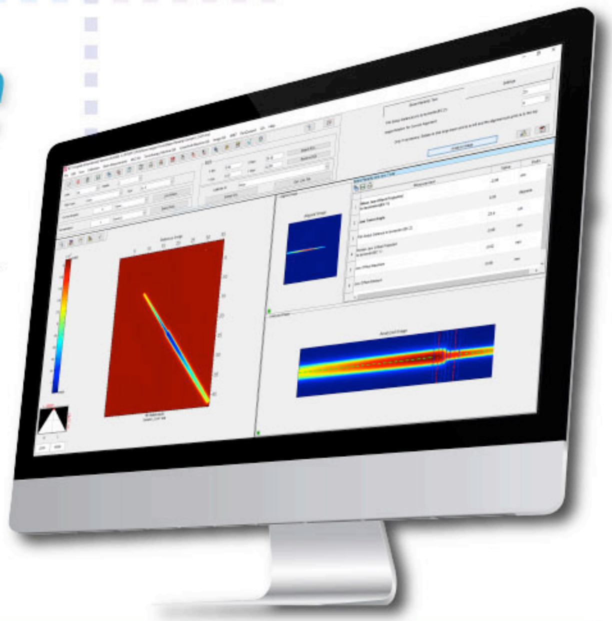

RIT *Complete* is the only RIT software package that offers the enhanced TomoTherapy® Registration feature. Easily perform exact dose comparisons for TomoTherapy® Patient QA using this automated technique.

All packages, RIT *Complete*, RITG135, and RITG148+, utilize a combination of powerful, robust routines in a user-friendly interface, which maximize the efficiency and precision of all measurements. For added convenience, users can easily create PDF reports for all routines and export their data to the RIT*trend*™ statistical database for large-scale analysis over time.

CLICK TO SCHEDULE A PERSONAL DEMO OF ANY PRODUCT PACKAGE

RADIOLOGICAL IMAGING TECHNOLOGY, INC.
RADIMAGE.COM®
+1.719.590.1077 x211 // sales@radimage.com

Connect with RIT
@RIT4QA